

Original papers

Automated robust crop-row detection in maize fields based on position clustering algorithm and shortest path method



Xiya Zhang, Xiaona Li, Baohua Zhang*, Jun Zhou, Guangzhao Tian, Yingjun Xiong, Baoxing Gu

College of Engineering, Nanjing Agricultural University, Nanjing 210031, Jiangsu, PR China

ARTICLE INFO

Keywords:

Crop row detection
Position clustering algorithm
Shortest path method
Linear regression
Autonomous navigation
Machine vision

ABSTRACT

Crop row detection is critical for precision agriculture and automatic navigation. In this paper, a novel automatic and robust crop row detection method is proposed for maize fields based on images acquired from a vision system. As the image quality is easily affected by weed pressure and gaps in the crop rows, the proposed method was designed with the required robustness in order to deal with these undesirable conditions, and it consists of three sequentially linked phases: image segmentation, feature points extraction, and crop row detection. The image segmentation is based on the application of a modified vegetation index and double thresholding combining the Otsu method with the particle swarm optimization, thus achieving a separation between the weeds and crops. During the procedure of crop row detection, the position clustering algorithm and shortest path method were applied successively to confirm the final clustered feature point set. Finally, a linear regression method based on least squares was employed to fit the crop rows. The experimental results show that the detection accuracy of this proposed method is 0.5°, which out-performs the classical approach based on the Hough transform.

1. Introduction

Automatic detection of crop rows in natural fields is essential for precision farming and automatic navigation and for agricultural robots. It has a wide range of applications such as planting, fertilization, plant protection, weeding, and harvesting (Jiang et al., 2015). With accurately detected crop rows from the camera images, these processes can be easily automated by guiding an autonomous vehicle according to the detected rows (Vidović et al., 2016). Obviously, automatic navigation is quite beneficial as it would reduce the operator fatigue and improve the vehicle positioning accuracy, which would lead to higher productivity (Gerrish et al., 1997). Therefore, the development of reliable and real-time crop row detection methods is of great significance in the field of precision farming.

This important issue primarily concerns crop-row and weed detection, which has attracted much attention (Montalvo et al., 2012). Different imaging-based methods have been used for detecting crop rows (García-Santillán et al., 2017a). Typically, these methods fall into a few categories according to their detection principle, such as Hough transform (HT), linear regression, blob analysis, stereo vision, and horizontal strips.

The Hough (1962) is one of the most commonly used machine vision methods for identifying crop rows (Slaughter et al., 2008). It is a

feature extraction technique used in digital image processing, image analysis, and computer vision (Duda, 1972). The core concept of the HT is the accumulation of the votes and detection of the peaks in the parameter space. In order to speed up the calculation, Xu et al. (1990) proposed a randomized HT (RHT) algorithm. The special idea involved in locating lines with the RHT is that it randomly selects two edge pixels each time with equal probability in the image space. However, high weed pressure and serious crop loss would cause the incorrect detection of the lines or even inability to detect the lines.

The linear regression method was used to detect lines fitted to outliers as a method of identifying the crop-row guidance information (Billingsley and Schoenfisch, 1997). In addition, Søgaard and Olsen (2003) located barley crop rows using weighted linear regression. This is a feasible approach that is applicable when pixels of crop rows are well separated from those of the weeds. Moreover, Montalvo et al. (2012) and Guerrero et al. (2013) predicted the expected position of the crop rows and then adjusted the position through the Theil-Sen estimator. However, its effectiveness is highly affected by the pixels of the weeds. Therefore, linear regression is only feasible if the pixels of the weeds and crops have been separated.

The blob analysis method is used to identify and characterize regions of contiguous pixels of the same value in a binaries image (Fontaine and Crowe, 2006). The gravity centers of these regions

* Corresponding author.

E-mail address: bhzhang@njau.edu.cn (B. Zhang).

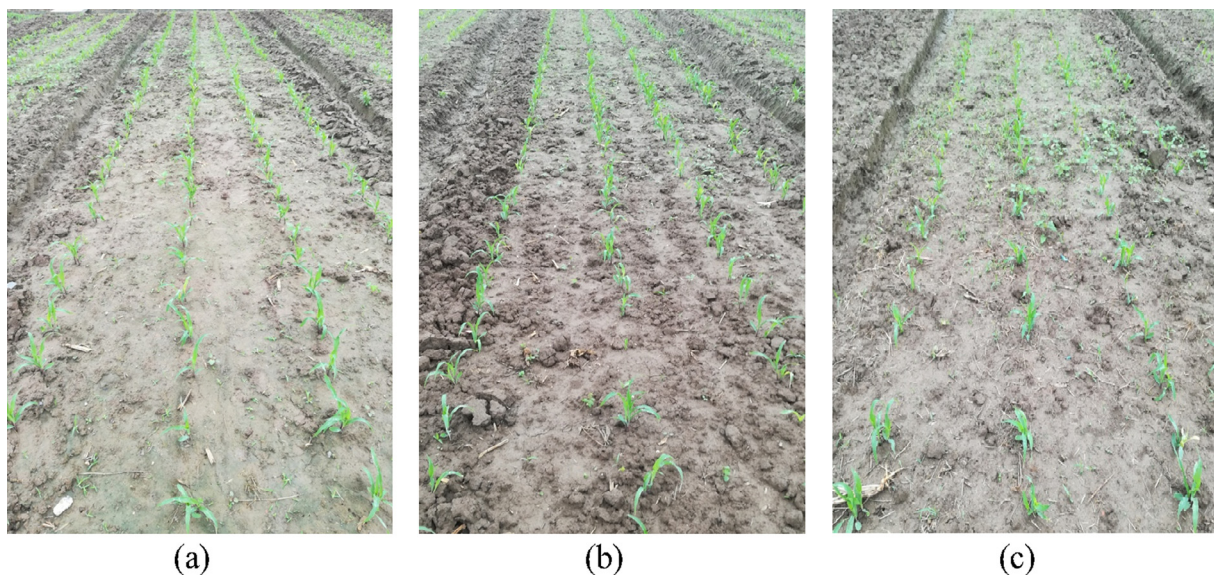


Fig. 1. Original images with various weed distribution situations: (a) low weed pressure, (b) presence of gaps, and (c) high weed pressure.

determine straight rows by associating an equation with each crop row (García-Santillán et al., 2017a). Based on these associations and the direction and displacement of the tractor, crop rows were detected (Burgos-Artizú et al., 2011; Bengochea-Guevara et al., 2012). Jiang et al. (2015) presented an algorithm based on small regions of interest and least squares fitting while taking into consideration known inter-row spaces in fields of wheat, corn, and soybean. However, this algorithm does not distinguish between blobs caused by weeds and crops well in weedy areas.

The stereo vision method is usually used when the heights of the weeds and crop plants above ground are highly visible and when the weed and crop plants differ in height (Romeo et al., 2012). Kise and Zhang (2008) developed a stereo-vision-based crop-row tracking navigation system for agricultural machinery. Stereo-image processing is used to determine the 3D position of the field of the object of interest from the obtained stereoscopic image. Furthermore, Rovira-Más et al. (2008) applied precision vision to other areas of precision agriculture. However, this method is only feasible if the crop or weeds in the 3D scene have relevant heights.

The horizontal strips method determines crop rows through image analysis without segmentation. Søgaard and Olsen (2003) firstly divide the color image into its red, green, and blue channels and then extract the living plant tissue by applying well-tested methods (Woebbecke et al., 1995). Lastly, after the transformation, the gray-level images are divided into 15 horizontal strips, and the vertical sum of the gray values for each strip are calculated. Moreover, Sainz-Costa et al. (2011) developed a strategy for identifying crop rows based on the analysis of video sequences. The above methods work well in the case of low weed pressure. However, in complex conditions comprising high pressure or a severe shortage of available images, the strip features generally cannot be detected accurately.

However, as mentioned above, it is obvious that complex outdoor agricultural environments have a significant influence on the image processing. Gaps may appear in the crop rows owing to a lack of germination, the occurrence of defects, or the presence of pests/diseases during planting. Different plant heights and volumes are mapped under image perspective projection with different widths (García-Santillán et al., 2017b). In addition, a high ratio of weed density with spectral components of similar color to crops can be present in the inter-row spaces and close to the real crop rows, thus resulting in false widths in the imaged crop rows and, hence, fake crop rows during detection (García-Santillán et al., 2017a).

While extending the advantages of the existing methods described above, we design a new crop row detection method that can cope with complicated conditions with a focus on weed pressure and crop gap treatment. The designed automation method comprises three main modules: image segmentation, feature point extraction, and crop row detection. In the first module, a modified vegetation index and double thresholding combining the Otsu method with the particle swarm optimization (PSO) method were used to obtain a good segmentation result. Subsequently, the vertical projection method is applied to divided horizontal strips in order to extract the feature points that indicate the crop row centers. The clustered point sets are then obtained based on the position clustering algorithm and shortest path method. Lastly, the crop rows are detected using least squares fitting. Therefore, the main contributions of this paper are the creation of a new vegetation index and optimization of the double thresholding method to improve the effect of segmentation; in addition, we apply the position clustering algorithm and shortest path method in order to make the least squares method (LSM) feasible, which further improves the robustness of the method.

2. Materials and methods

2.1. Image acquisition

Maize crop images in the seedling stage were selected in this study. A Samsung S850 color camera was mounted on a farm vehicle and the 300 images were captured during May 2017 in the same maize fields in the countryside. The proposed algorithm is developed using Microsoft Visual C++ 6.0 and the free computer vision library OpenCV 1.0. Furthermore, the digital images were stored as 24-bit color images with resolutions of 3264×2448 pixels and saved in RGB (red, green, and blue) color space in the JPEG format. Camera setting was: pitch and roll angles of 30° and 0° with the camera placed at a height of 1.5 m from the ground. In order to reduce the amount of calculation required, sample processing is performed on the image by applying a pixel area relationship resampling method. As this method can prevent the occurrence of ripples when the image is zoomed out. Subsequently, the image size is shrunk to 793×595 pixels. In addition, Fig. 1 displays three illustrative examples at different growth environments of maize in conditions comprising (a) low weed pressure, (b) the presence of gaps in crop rows, and (c) high weed pressure.

2.2. Image segmentation

2.2.1. Modifications to the vegetation index

In the processing of RGB images, the first step comprises greenness image segmentation. In order to distinguish between green plants (crops and weeds) and the background (soil, stones, shadows, etc.), the best method is the application of vegetation indices (Xiang and Tian, 2011). Therefore, various vegetation indices have been designed. The famous vegetation indices are as follows: *ExG*, i.e., excess green index (Woebbecke et al., 1995; Ribeiro et al., 2005), *CIVE*, i.e., color index of vegetation extraction (Kataoka et al., 2003), *VEG*, i.e., vegetative index (Hague et al., 2006), *ExGR*, i.e., excess green minus excess red index (Neto, 2004; Meyer and Neto, 2008), and *COM*, i.e., combined index (Guerrero et al., 2013). After comparing the above indices, the *ExG* index was selected because of its outstanding performance and simplicity (Woebbecke et al., 1995; Montalvo et al., 2012). The following are the operations for extracting the *ExG* vegetation index.

In an RGB image, the red, green, and blue values, by default, range from 0 to 255. These values have to be normalized in order to calculate the chromatic levels and, thus, obtain the normalized spectral *r*, *g* and *b* components in the range of 0–1. These are estimated as follows (Montalvo et al., 2012):

$$r = \frac{R'}{R' + G' + B'}, g = \frac{G'}{R' + G' + B'}, b = \frac{B'}{R' + G' + B'}, r + g + b = 1 \quad (1)$$

The values of *R'*, *G'* and *B'* in formula (1) are the normalized RGB coordinates in the range of [0, 1] and are obtained as follows:

$$R' = \frac{R}{R_m}, G' = \frac{G}{G_m}, B' = \frac{B}{B_m} \quad (2)$$

where $R_m = G_m = B_m = 255$ for the 24-bit color images in this study.

The index *ExG* is computed as follows:

$$ExG = 2g - b - r \quad (3)$$

Furthermore, Romeo et al. (2012) applied a fuzzy clustering strategy to the pixels by analyzing the RGB components of the cluster, and the study shows that the green spectral components are dominant among the three spectral components and represent more than 36% of the other two components on average. Based in this, we multiply the value of *g* and *ExG* in order to highlight the green component of the plant pixel. Thus, a new vegetation index is obtained as *ExGG* = *ExG***g*. Similarly, *ExGG* is linearly mapped such that it ranges in the interval [0, 1] (Guerrero et al., 2013). Therefore, the difference between green plants and the background is enhanced, and the effect of the segmentation is outstanding.

2.2.2. Double thresholding combining the Otsu and PSO methods

Given the greyscale image after the *ExGG* application, the next step is its binarization for posterior processing. We have investigated different thresholding approaches (Otsu, 1979; Gée et al., 2008; Bossu et al., 2009; Montalvo et al., 2012) and found that double thresholding based on Otsu could be adapted to the highly changeable environmental conditions common in agricultural tasks because of its ability to dynamically self-adjust without learning (García-Santillán et al., 2017a). During double-thresholding processing, the Otsu adaptive threshold algorithm and the PSO are combined in this study. The basic idea of the Otsu method is to select an optimal threshold to divide the grey-level histogram of an image into two parts according to the principle of maximum intergroup variance. In addition, the following describes the principle of PSO.

In PSO, each particle can be considered as a candidate solution to the optimization problem, provided with a velocity and a position. In evolution, each particle updates its velocity and position according to tracking two extreme values: “individual extremum” and “global extremum”. The updating equations of the particle swarm are shown in

Eqs. (4) and (5).

$$v_{id}(t+1) = wv_{id}(t) + c_1rand(\cdot)(p_{id}(t) - x_{id}(t)) + c_2rand(\cdot)(p_{md}(t) - x_{id}(t)) \quad (4)$$

$$x_{id}(t+1) = x_{id}(t) + v_{id}(t) \quad (5)$$

where assuming a search in the *D*-dimensional space, the number of variables to be optimized here determines the dimension of the space *D*. The vector $x_i = (x_{i1}, x_{i2}, \dots, x_{iD})$ represents the position of the *i*-th particle, $v_i = (v_{i1}, v_{i2}, \dots, v_{iD})$ represents the velocity of the *i*-th particle, $p_i = (p_{i1}, p_{i2}, \dots, p_{iD})$ is the optimal position that the *i*-th particle has achieved thus far, $p_m = (x_{m1}, x_{m2}, \dots, x_{mD})$ is the optimal position of the current generation, $x_{id}(t)$ and $v_{id}(t)$ refer to the *d*-dimensional component of the position and velocity vectors, respectively, of the *i*-th particle in the *t*-th iteration, *w* is the inertia weight, *c*₁ and *c*₂ are the acceleration coefficients, and *rand*(·) is a randomly and uniformly chosen number from the interval [0,1].

Therefore, the Otsu method is regarded as the optimized objective function of the PSO. During the joint algorithm, the threshold is used as the particle, and each particle's fitness is calculated and compared with the optimal threshold. The optimized threshold is thus obtained. Here the variables are two thresholds, so the value of *D* is 2. During the process, the first thresholding was applied to separate the green plants (crops and weeds) from the background. The second thresholding was applied over the pixels representing the green plants, which facilitates a partial separation between the weeds and crops (García-Santillán et al., 2017b).

2.2.3. Morphological operations

After obtaining the initial binary image, an extra morphological dilation process is applied to expand the segmented plants. The dilation process can fill the gaps in the plants and the plants appear to comprise a greater number of green pixels (García-Santillán et al., 2017a). Subsequently, the aperture is filled through the flood water filling method, so that the white pixels representing the crops can be combined to form white spots. Then, the size of the area is used to represent the number of pixels included in the white spot. White spots with an area less than the threshold will be removed, whereas white spots with an area greater than the threshold will remain. This area constraint method is applied to eliminate insignificant small spots and spurious pixels from the binary image (although the crop row edges are also cleared at small areas, the position of the centerline of the crop row is not affected) (Si et al., 2010).

Fig. 2(a) displays the color space transformation on applying *ExGG* in Fig. 1(a). Green plants are identified as white pixels in Fig. 2(b) after the first thresholding. After applying the second thresholding, a number of weeds are eliminated, as shown in Fig. 2(c). Finally, Fig. 2(d) displays the results obtained after performing the morphological operations.

2.3. Feature points extraction

Prior to the estimation of the row positions, it is vital to determine the feature points that indicate the centers of the crop rows. In order to obtain such points, the binary image resulting from the above image segmentation is divided into a number of horizontal strips. In order to reduce the number of subsequent computations, each strip comprises more than one pixel row (Søgaard and Olsen, 2003). Let us assume that the division of the image into *N* strips is suitable.

Let binary image $Bw(i, j)$ ($i = 1, \dots, W$ and $j = 1, \dots, H$) be the grey value of the pixel at the position (i, j) , where *W* denotes the width of the image, and *H* denotes the height of the image. Let the size of each horizontal strip be $W \times h$, where *h* denotes the height of each strip and $h = H/N$, let $S_n(i)$ denote all the non-zero pixels of the *n*-th horizontal strip and the *i*-th column in the vertical projection direction, and let μ_n

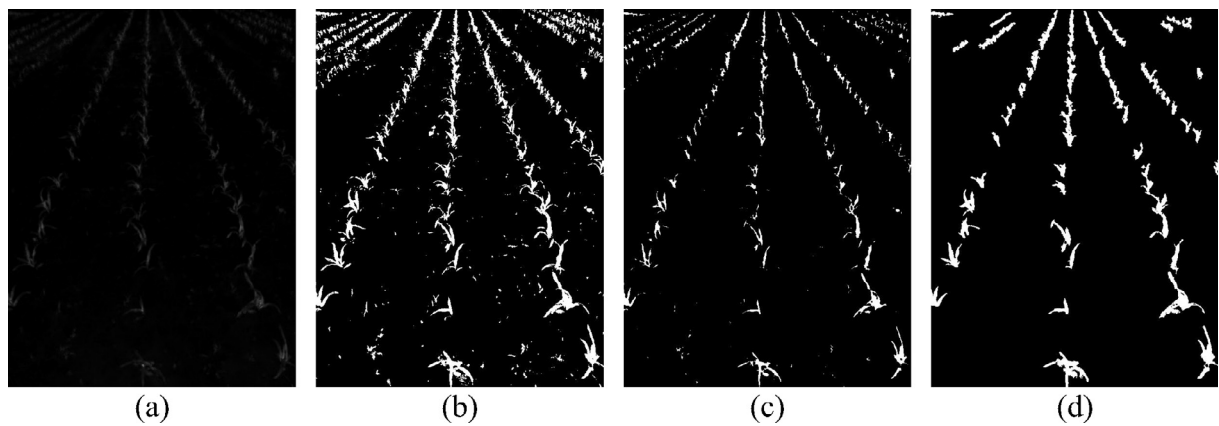


Fig. 2. Image segmentation process: (a) Vegetable index extracted from the image in Fig. 1(a); (b) binary image obtained after the first thresholding; (c) binary image obtained after the second thresholding; and (d) binary image obtained after the morphological operation.

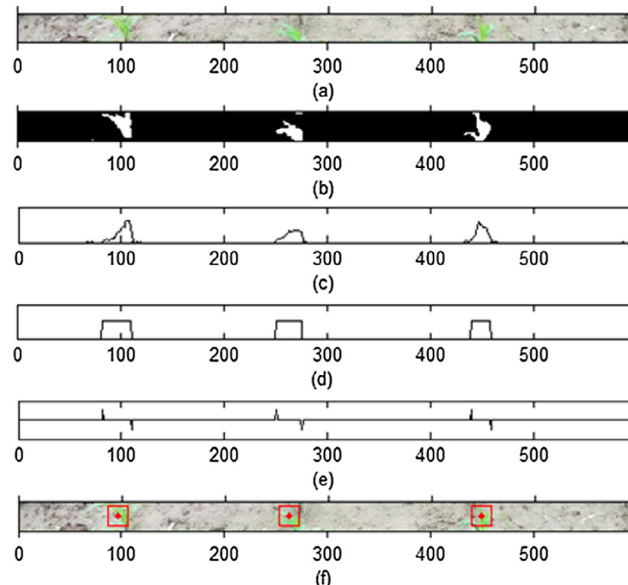


Fig. 3. Feature points extraction process in a horizontal strip: (a) Strip from original image; (b) strip from binary image; (c) vertical projection curve; (d) vertical projection curve after threshold; (e) differential curve; and (f) location feature point results.

denote the mean of S_n , as shown in Eqs. (6) and (7) (Jiang et al., 2015).

$$S_n(i) = \sum_{j=h(n-1)+1}^{hn} Bw(i, j) \quad (6)$$

$$\mu_n = \frac{1}{W} \sum_{i=1}^W S_n(i) \quad (7)$$

Mathematically, the process can be described as follows: the horizontal strips are scanned column-by-column such that n changes from 1 to N . In the processing of the n -th horizontal strip, $S_n(i)$ and μ_n are calculated firstly. Secondly, if $S_n(i) \geq \mu_n$, then $S_n(i) = 1$; otherwise $S_n(i) = 0$. Thirdly, the differential function $Diff_n(i)$ of the projection curve after the threshold processing is calculated. Fourthly, the left and right edge points of the crop row are determined: if $Diff_n(i) > 0$, the column comprises the rising point (the left edge of the crop row); if $Diff_n(i) < 0$, the column comprises the falling point (the right edge of the crop row). The detailed information about vertical projection method can be found in the literature of Jiang et al. (2008). Finally, the midpoints of the rising and falling points are calculated, which is the abscissa of the candidate feature point of the crop row, and the middle point of the ordinate of the horizontal strip serves as the ordinate of the feature point. In addition, in order to extract the feature points that represent the center of the crop row, when the distance between the adjacent rising point and falling point is less than a width threshold (11 pixels in our research), we regard it as noise and remove that point (Jiang et al., 2009). Fig. 3 displays the process of feature point location in a horizontal strip based on the vertical projection method.

Similarly, in order to dynamically detect the number of rows of the current image crop row, a vertical projection strategy is also adopted.

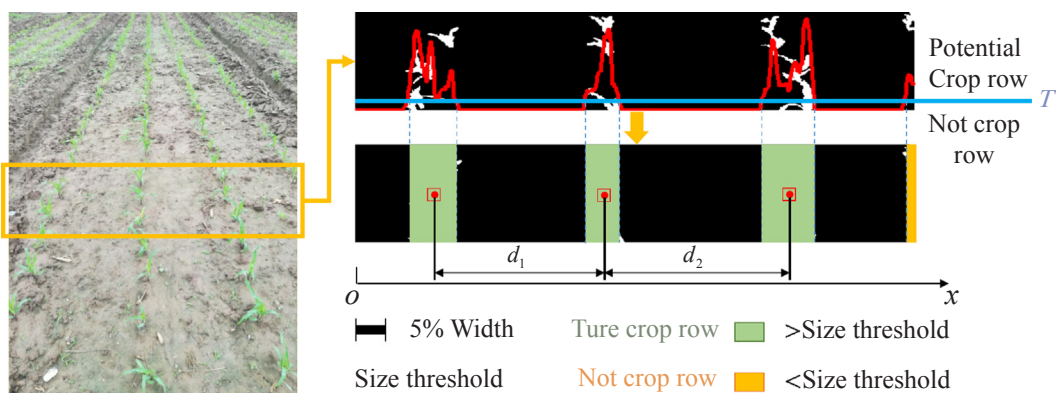


Fig. 4. Crop row quantity detection process. The result is the number of true crop rows (green bar) with a width greater than 5% of the image width. (For interpretation of the references to colour in this figure legend, the reader is referred to the web version of this article.)

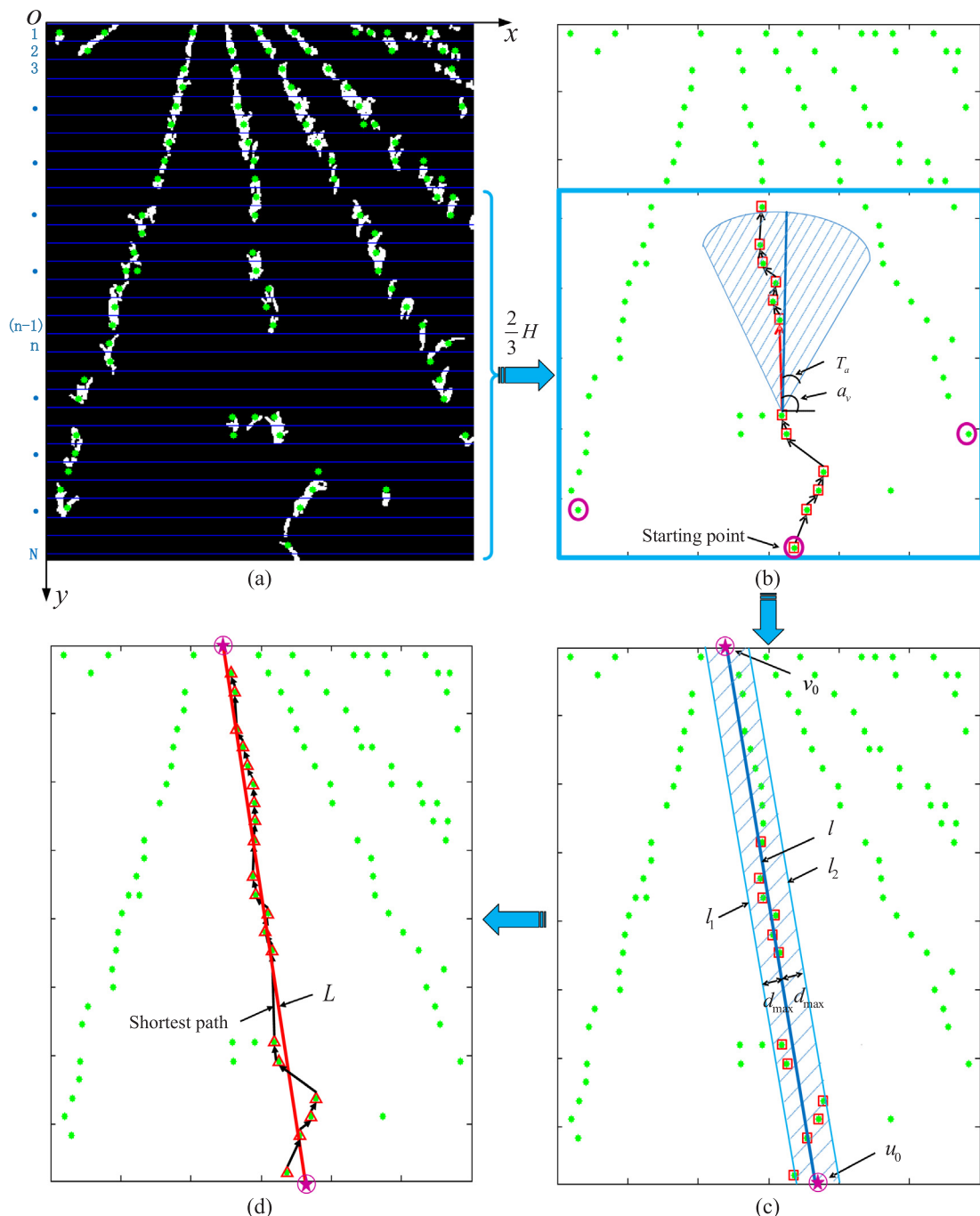


Fig. 5. Crop row detection process of Fig. 1(b): (a) Horizontal strips are divided by blue line; (b) the current points of the 2/3 of the bottom part of the image is represented in red (\square); (c) the initial clustered points are indicated by the blue hatched area; (d) the final clustered points are indicated using red (\triangle), the fitted crop row is represented by a red line, and all the feature points are represented using green (\circ). (For interpretation of the references to colour in this figure legend, the reader is referred to the web version of this article.)

The image is equally divided into five parts, and the value of $W \times h^*$ of the image is intercepted at the middle position in the image height direction, where $h^* = H/5$. Only when the vertical projection curve is above the threshold T , it is considered as a potential crop row. And this threshold is equal to the mean value as described above, i.e. $T = \mu$. After this, the potential crop rows are identified as true crop rows if the distance between the adjacent rising point and falling point is higher than 5% of the image width (30 pixels in this case) (Burgos-Artizzu et al., 2011). In Fig. 4, all the steps in the procedure are illustrated and the parameters d_1 and d_2 represent the distance between adjacent true crop rows. The quantity of true crop rows is represented by N_{row} .

2.4. Crop row detection

2.4.1. Position clustering algorithm

After obtaining the feature points, the next goal is to assign the points to each crop row. In order to determine which feature points participate in the parameter estimation for each crop row, we resort to the position clustering algorithm.

The clustering analysis is applied widely to confirm the real feature points indicating crop rows according to the distance relationship between the feature points and estimated crop line. However, as crop rows are often accompanied by weed pressure and crop gaps, the results

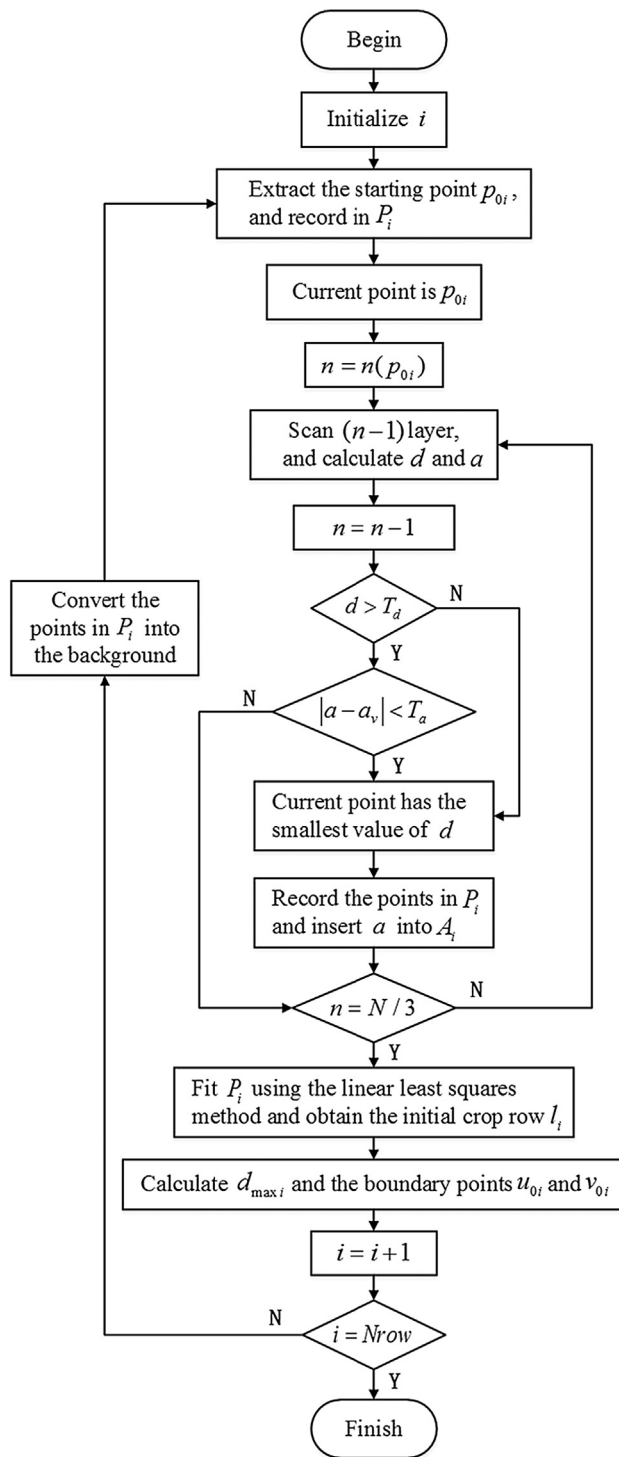


Fig. 6. Position clustering algorithm flow chart.

obtained on using this clustering method are not satisfactory. In view of the above problems, we propose a position clustering algorithm that combines the distance constraints with angle constraints between the feature points. At positions closer to the top of the image, the distance between the rows of the crops is smaller, thus resulting in a close spacing of the feature points. We therefore judge the overall trend of the crop row by processing the 2/3 of the bottom part of the image. During the processing, the feature point for which the distance is less than the threshold is collected first. If the distance exceeds the threshold, the feature point of which the angle matches the overall trend is also collected. Subsequently, the initial fitting of the obtained

point set gives the overall trend of the crop line, and the fitting line is then expanded in parallel to obtain the initial clustered point set. In this manner, the impact of the weeds and crop gaps on the identification of real crop rows decreases significantly.

Before implementing the algorithm, the starting point of each line is required to be determined. It is known that the number of crop rows is N_{row} , and the image is evenly split into N_{row} blocks by columns. The feature point image is scanned from bottom to top and from left to right in each block. The first feature point scanned by each block is the starting point for each crop row. This position clustering algorithm flow chart is shown in Fig. 6. Furthermore, the specific position clustering algorithm is as follows:

- (1). The crop row counter i is initialized; let d denote the distance between the feature point and the current point, let a denote the angle between the positive direction of the x -axis and the line connecting the current point and feature point, let P_i denote a set of feature points of the i -th crop row, let A_i denote the accumulator of the angle a of the i -th crop row, let a_v denote the average of A_i , let T_d denote the distance threshold, let T_a denote the angle threshold, and let p_{0i} denote the starting point of the i -th crop row.
- (2). On extracting the starting point p_{0i} as the current point, it is inserted into set P_i .
- (3). This point p_{0i} belongs to the $n(p_{0i})$ -th layer of horizontal stripes. Let $n = n(p_{0i})$.
- (4). All the feature points of the $(n-1)$ layer are scanned horizontally; let $n = n-1$, and the distance d and angle a are calculated. If there are points whose distance d is less than or equal to T_d , skip to step (5). If all the distances are greater than T_d , move to step (4) as this indicates that the crop row has a gap in the n -th layer.
- (5). If $|a - a_v| < T_a$, move to step (5), which indicates points meeting this condition matches the overall trend; else, skip to step (6).
- (6). Let the feature point with the smallest value of d be the new current point, let this point be inserted into set P_i , and insert the angle a into set A_i .
- (7). It is determined whether n is equal to $N/3$. If not, skip to step (3); else, the position clustering algorithm of the i -th row is completed, and then P_i is fit using the linear least squares method, and the initial crop row l_i is obtained. The intersection of l_i with the four edges of the image is calculated, and two boundary points u_{0i} and v_{0i} are obtained. The maximum distance from all the feature points in P_i to l_i is calculated and denoted as $d_{max,i}$.
- (8). Let $i = i + 1$, and if the current crop row counter i is equal to N_{row} , the program is terminated; else, the points in the current set P_i are converted into background points, and we skip to step (2) to continue the execution.

In this manner, during each crop row processing, an initial crop row l , the maximum distance d_{max} , and the boundary points u_0 and v_0 are obtained. Subsequently, in order to obtain the initial feature point set for each crop row, two straight lines l_1 and l_2 are constructed, which are parallel to the left and right sides of l respectively, and their vertical distance from l is d_{max} . This determines a bar area as indicated by the hatched line in the image space in Fig. 5(c). All the feature points in this area are clustered into set P^* , which is the initial clustered point set.

2.4.2. Shortest path method

In order to reduce the occurrence of the phenomenon owing to which the pseudo feature points (weeds, etc.) are concentrated on the side of the real crop line, which results in a deviation in the detected crop lines, we re-screen the initial clustered point set. Taking advantage of the above intersection points u_0 and v_0 as the starting and ending points, a shortest path is used to filter the feature points close to the real crop row. It is clear that Dijkstra's algorithm can be used to calculate the shortest path between two points (Dijkstra, 1959). However, its time complexity is high, and a great amount of calculation is required.

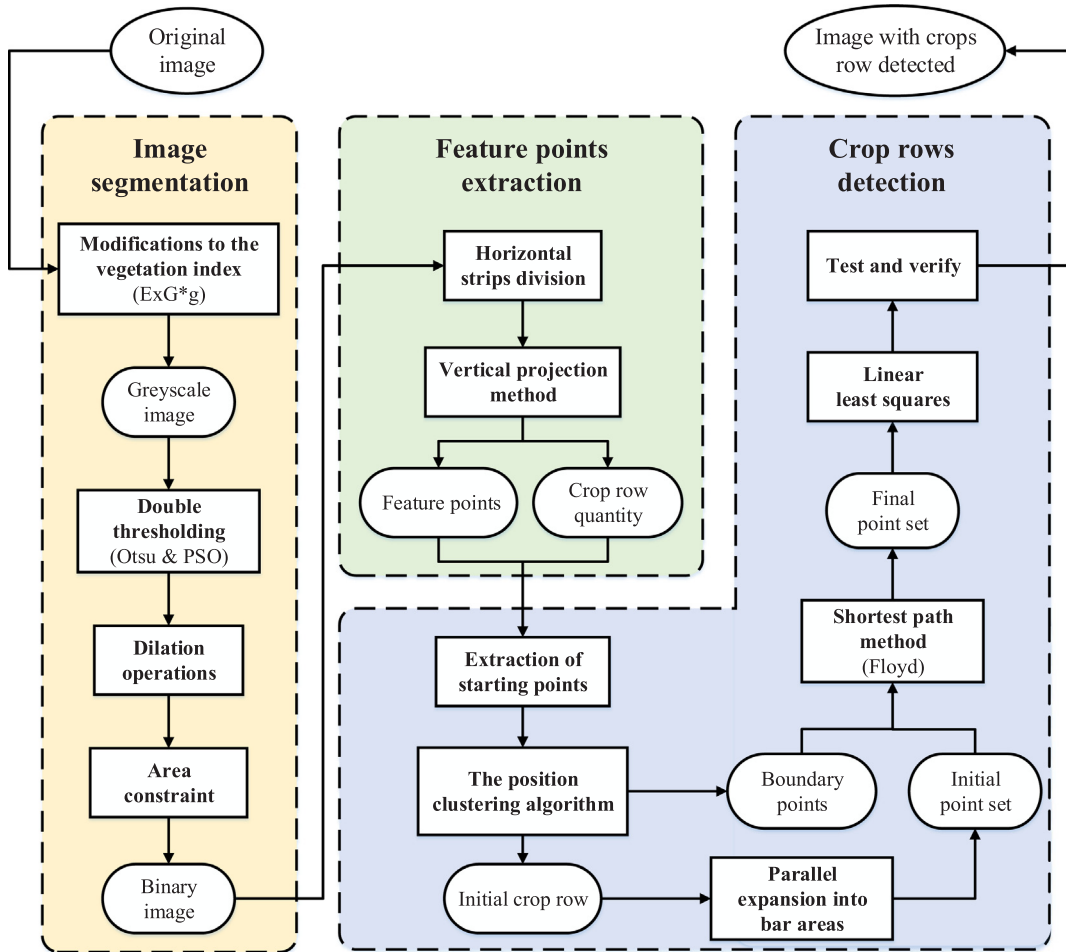


Fig. 7. Flowchart of the entire detection algorithm.

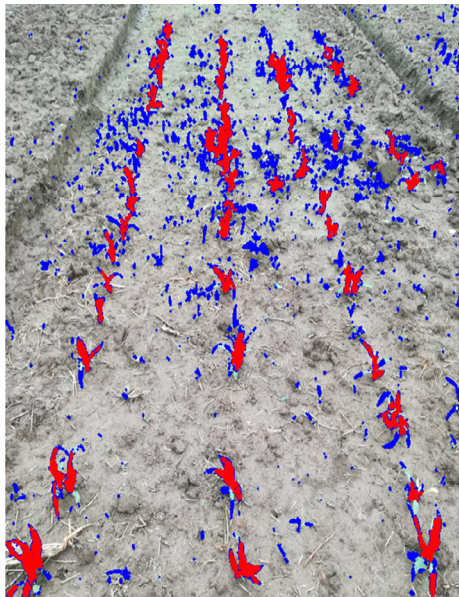


Fig. 8. Segmented image identified using the proposed method (red) and the Otsu method (blue) respectively. (For interpretation of the references to colour in this figure legend, the reader is referred to the web version of this article.)

Therefore, in this paper, the Floyd algorithm is applied instead (Floyd, 1962).

Prior to this, it is necessary to rearrange the initial clustered feature points. According to the order of the original layers of the feature points, they are arranged again from small to large, such that the order of their layers is adjacent. This eliminates the effects of discontinuities in layer order caused by crop row gaps.

Now, given the initial clustered point set P^* , let us suppose it has m points. A weighted graph $G = (P^*, E, D)$ is then constructed, wherein $P^* = \{p_1, \dots, p_m\}$ and p_1, \dots, p_m denote the initial clustered feature points, where E denotes a collection of edges and where $D = (d_{ij})_{m \times m}$ denotes an adjoining matrix. If points P_i and P_j are in adjacent layers, then let d_{ij} denote the distance between them; otherwise let d_{ij} be infinite.

$$D = \begin{bmatrix} d_{11} & d_{12} & \dots & d_{1m} \\ d_{21} & d_{22} & \dots & d_{2m} \\ \vdots & \vdots & \vdots & \vdots \\ d_{m1} & d_{m2} & \dots & d_{mm} \end{bmatrix} \quad (8)$$

$$d_{ij} = \begin{cases} p_i \text{ distance from } p_j & , |n(p_i) - n(p_j)| = 1 \\ \infty & , |n(p_i) - n(p_j)| \neq 1 \end{cases} \quad (9)$$

$$d_{ii} = 0 \quad i = 1, 2, \dots, m \quad (10)$$

The basic idea of the Floyd algorithm is to recursively generate a matrix sequence $D_1, \dots, D_k, \dots, D_m$, in which the element $D_k(i, j)$ of the i -th row and the j -th column of the matrix D_k represent the shortest path of which the point number that passes through the path from p_i to p_j is not greater than k (Si & Sun, 2015). The iterative formula is as follows:

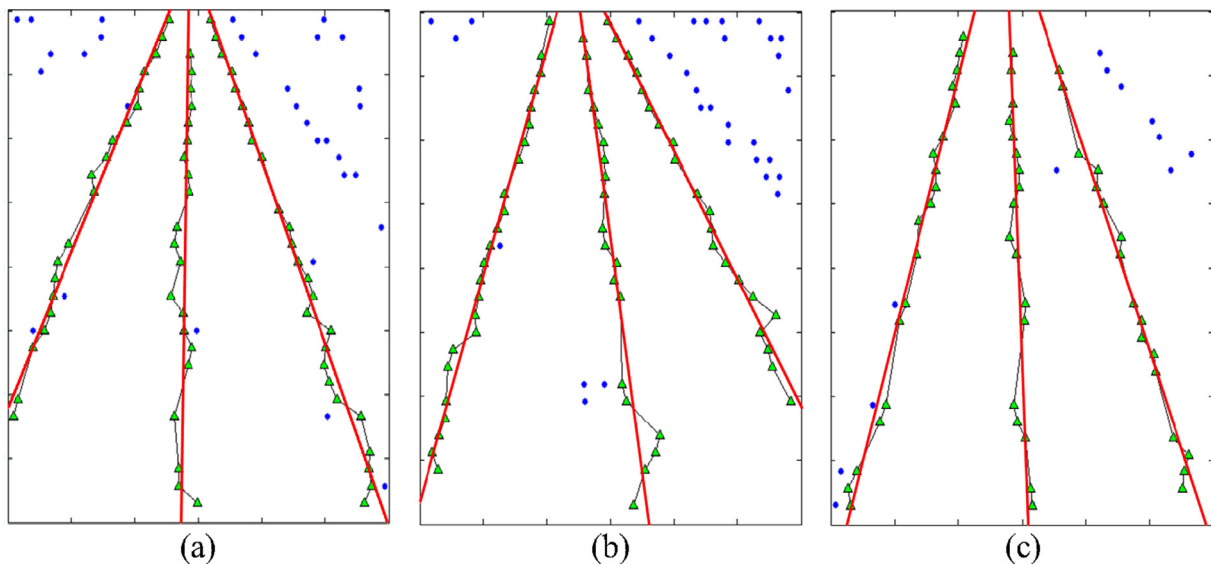


Fig. 9. Result of final clustered points (Δ) and the fitted straight line (red) in Fig. 1. (For interpretation of the references to colour in this figure legend, the reader is referred to the web version of this article.)

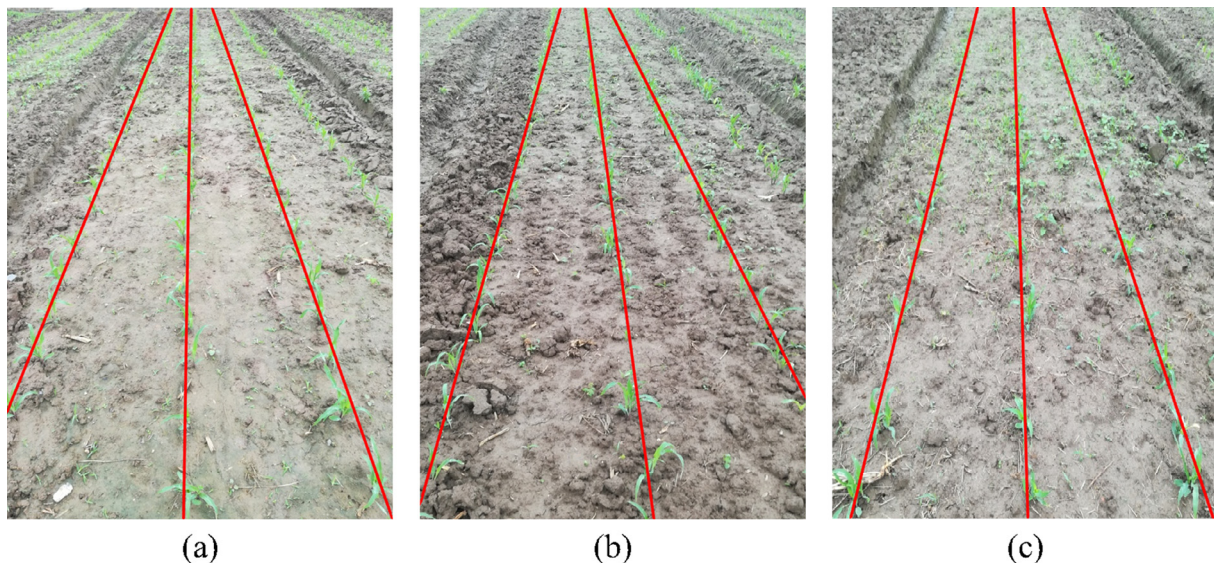


Fig. 10. Result of crop rows detection in Fig. 1.

$$D_k(i, j) = \min(D_{k-1}(i, j), D_{k-1}(i, k) + D_{k-1}(k, j)), \quad i, j, k = 1, 2, \dots, m \quad (11)$$

where k is the number of iterations. When $k=m$, we can obtain the point set of the shortest path between u_0 and v_0 . Therefore, the final clustered point set P^{**} is obtained.

After determining the final feature point set indicating the crop rows, now the problem has been reduced to assign the corresponding straight-line equation to each crop row. We thus use methods that are based on regression analysis. In this study, the LSM is applied to find the straight line that best fits a given set of points by minimizing the sum of the squares of the offsets of the points from the straight line. Fig. 5(d) shows the final clustered feature points (Δ), shortest path (black fold line), and fitted crop row (red line). In conclusion, the flowchart of the entire detection algorithm is shown in Fig. 7.

3. Results and discussion

3.1. Image preprocessing

In order to detect the performance of the proposed algorithm under various weed distribution conditions, several representative images of maize fields were randomly selected for processing in this work. Fig. 1(a) displays the image of a field with low weed pressure; Fig. 1(b) displays the image of a field with incomplete row structures owing to missing plants; and Fig. 1(c) displays the image of a field that has high weed pressure.

Firstly, from the above images shown in Fig. 2(a), it can be observed that after the green value is emphasized by multiplying it by g , the green plants including the crops and weeds were identified from the original color images of the corresponding images in Fig. 1(a). Subsequently, the greyscale image in Fig. 2(a) was segmented with double thresholding by combining the Otsu with PSO methods; after the second thresholding, the crop plants were identified, and a binary image was obtained in Fig. 2(c), where potential crops and the rest respectively

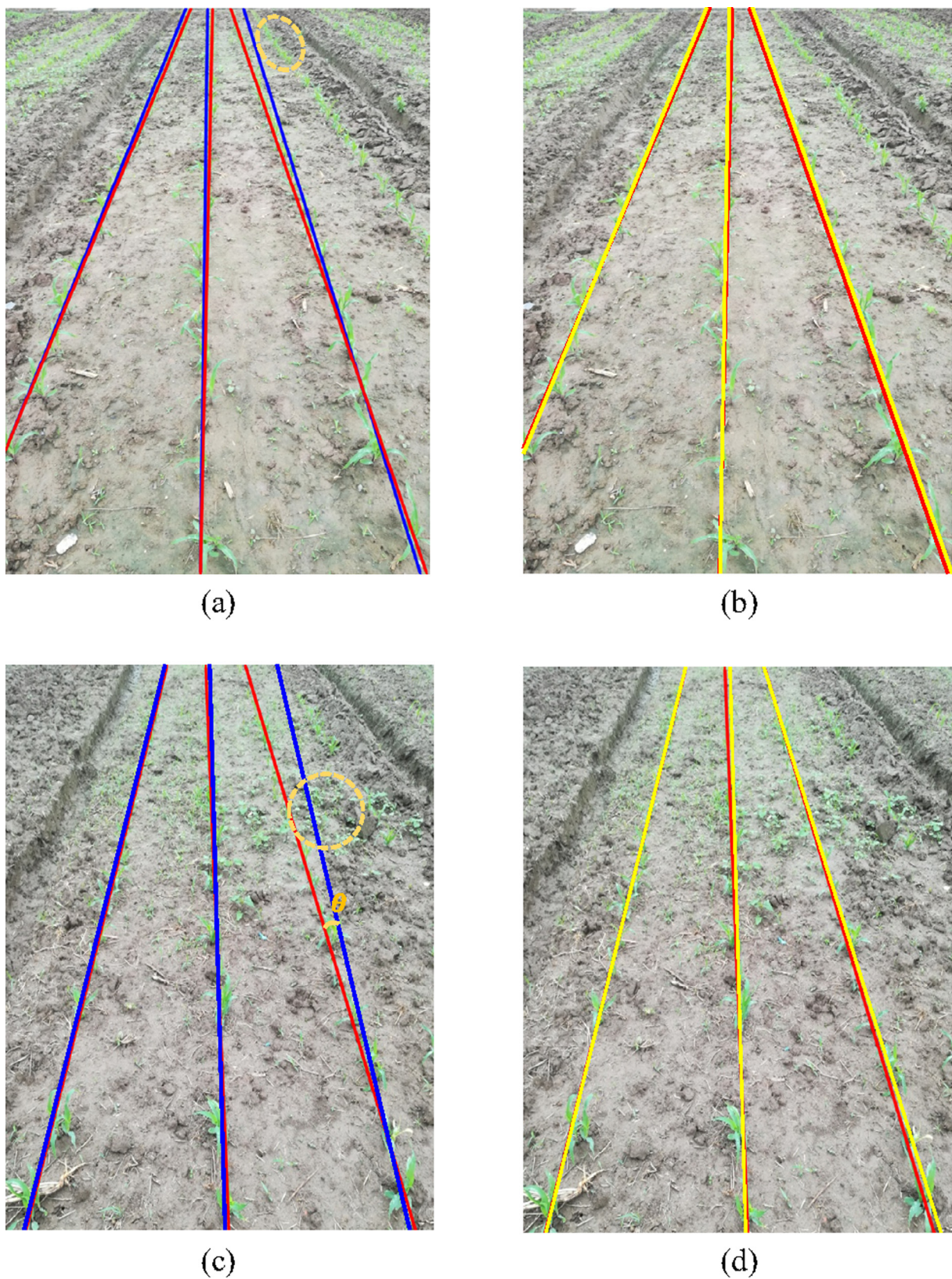


Fig. 11. Comparison of detected crop rows and real rows. Blue lines were obtained using HT, yellow lines were obtained on using the proposed method, and red lines were drawn by expert human. (a) and (b) show the crop rows for low-density weeds; and (c) and (d) show the crop rows for high-density weeds. (For interpretation of the references to colour in this figure legend, the reader is referred to the web version of this article.)

Table 1

Linear parameters of various methods for various weed pressures.

Linear parameters	Low-density weeds with our method	Low-density weeds with HT	High-density weeds with our method	High-density weeds with HT
k (left)	−2.4417	−2.4487	−4.0301	−4.0104
b (left)	622.5198	620.3047	906.9036	906.3724
x_{top}	284.7481	283.3042	282.0705	279.2361
x_{bottom}	273.8883	273.4866	284.6071	284.0896
k (right)	2.8402	3.1927	3.1826	4.2592
b (right)	−898.1594	−1064.5999	986.4865	1608.6400

Table 2

Detection accuracy of various methods for various weed pressures.

Detection accuracy (°)	Low-density weeds with our method	Low-density weeds with HT	High-density weeds with our method	High-density weeds with HT
θ (left)	0.4941	0.5516	0.0614	0.0044
θ (middle)	0.4303	0.5056	0.5176	0.3502
θ (right)	0.2466	1.7587	0.6641	4.2302
θ (average)	0.3903	0.9386	0.4144	1.5283

appear as white and black pixels. As expected, double thresholding was not affected by the weed pressure and soil background. Then, the morphological dilation process and the area constraint eliminate smaller areas, so that the disturbance caused by the weed noise can be reduced. Furthermore, the area threshold is influenced by the stage of the crop growth. Practical experience has shown that 200 is suitable for our study. Finally, the last pre-processed image was obtained and shown in Fig. 2(d).

Therefore, a series of image segmentation methods were established. Fig. 8 shows the results of two segmentation methods applied to Fig. 1(c). The blue pixels in Fig. 8 represent the green plants (crops and weeds) based on the classic Otsu method, and the potential crops based on our method are indicated in red. It is obvious that our method can better extract the crops even if the weed pressure is extremely high in the image in Fig. 1(c). This means that the proposed segmentation methods are appropriate for high weed densities and improves the accuracy of the posterior crop-row detection.

3.2. Identification of the center line of crop rows

As shown in Fig. 5(a), the image was divided into a number of horizontal strips to extract the feature points. Therefore, the number of horizontal strips directly influenced the velocity and precision of our approach. Extensive tests also showed that 30 horizontal strips can provide a good result for a wide variety of conditions. Since the total height of the image is 793 pixels in our research, we take the top 29 horizontal strips with a height of 27 pixels, and the bottom horizontal strip has a height of 10 pixels.

In addition, it should be pointed out that owing to the introduction of the two parameters of distance threshold and angle threshold, the position clustering algorithm becomes capable of dealing with incomplete row structures that are present owing to the missing plants in Fig. 5(b). The distance threshold T_d is the average of the distance between adjacent feature points in the center of the image, i.e. $T_d = (d_1 + d_2)/2$ in Fig. 4, and an angle threshold T_a of 30° is suitable for our study.

Afterwards, Fig. 5(d) shows that the pseudo feature points are excluded and do not participate in the parameter estimation of the straight line, thus contributing to more precise straight-line adjustments. All of this can be attributed to the shortest path method, which extracts the feature points closest to the real crop line and excludes the points considered as outliers from the estimate. Therefore, this method

exhibits outstanding performance under high weed-pressure conditions.

Subsequently, the least squares method (LSM) is applied to obtain the final crop line. In the LSM, as the squares of the offsets are used, the outlying points usually have a disproportionate effect on the fit, which may cause an undesirable result. However, in the position clustering, the feature point range has been controlled in the bar band shown in Fig. 5(c), and thus, no singularity points appear in the final clustered point set. Finally, the application of the LSM meets our expected result. Fig. 9 displays the shortest path for Fig. 1, and Fig. 10 displays the final result of crop row detection based on the use of LSM for Fig. 1.

In order to detect the real crop rows in the image, we have also compared the performance of the proposed method with that of the HT (Slaughter et al., 2008). The comparison is established in terms of accuracy, and the accuracy is measured based on the expert human criterion, where a line is considered desirable if the angle between the detected straight line and the real crop row is sufficiently small (ignoring the parallel case). Thus, the deviation angle θ between the detected crop row and the real crop row indicates the accuracy of the detection shown in Fig. 11(c) (Jiang et al., 2015). Fig. 1(a) (low-density weeds) and (c) (high-density weeds) are two representative examples of our selection, and the tested results of two types of algorithms are shown in Fig. 11. The linear parameters obtained by different methods are shown in Table 1. In Table 1, k denotes the slope, b denotes the intercept, x_{top} denotes the abscissa of the intersection of the centerline and the top of the image, and x_{bottom} denotes the abscissa of the intersection of the centerline and the bottom of the image. Table 2 shows the detection accuracy for the various detection methods for various weed pressures.

As can be observed from Fig. 11, the straight line obtained on using our algorithm (yellow lines) and HT (blue lines) all fit closely with the actual crop row (red lines) in the left and middle which the deviation it is less pronounced. However, in the right row, the huge deviation produced by the HT is due to the presence of adjacent green plants (marked with the orange dotted circle), which have been considered during the procedure of estimation. In conclusion, both the proposed algorithm and the HT method can be used to accurately identify the center line of the crop rows when the other green plant is far from the crop row. However, when other green plants are close to the real crop lines, the accuracy of the HT decreases, and the proposed algorithm can still accurately identify the center line of the crop rows. In addition, according to Table 2, the average deviation angle obtained by our method is always smaller than the one obtained by HT, either under the conditions of high-density weeds or low-density weeds. Therefore, it is clear that the proposed algorithm has superior performance over HT in terms of detection accuracy.

4. Conclusion

In this paper, we propose a novel method for the accurate crop-row detection in maize fields. The proposed method is based on three main processes: image segmentation, feature point extraction, and crop row detection. First, the original images were captured in the RGB color space and transformed into grey images on applying the *ExGG* vegetation index. Subsequent to this transformation, double thresholding combining Otsu with PSO and morphological operations facilitated the separation of the weeds and crops. Then, the vertical projection method was combined with horizontal strips division to identify the feature points of the crops. The position clustering algorithm and shortest path method were applied to confirm the final clustered feature point set, thus making an important contribution to the estimation of points that indicate the center lines of the crop rows. Finally, the LSM is applied to fit the line equation corresponding to the crop row. The performance of the proposed method is tested using a set of images, and this experiment results show that the deviation angle of the algorithm is less than 0.5°. As a result, we verified that the method proposed in this paper outperforms the HT in terms of accuracy based on a qualitative and

quantitative analysis. In the next stage, we will focus on the optimization of processing time.

Acknowledgements

This work was supported by The National Key Research and Development Program of China (project No. 2017YFD0700500), the Key Research and Development Program of Jiangsu (project No. BE2017370) and the Fundamental Research Funds for the Central Universities (project No. KYGX201701).

Appendix A. Supplementary data

Supplementary data to this article can be found online at <https://doi.org/10.1016/j.compag.2018.09.014>.

References

- Bengochea-Guevara, J.M., Conesa-Muñoz, J., Ribeiro, Á., 2012. Developing a small autonomous robot for crop inspection. In: Information Technology, Automation and Precision Farming. International Conference of Agricultural Engineering-CIGR-AgEng 2012: Agriculture and Engineering for a Healthier Life, Valencia, Spain, 8–12 July 2012. CIGR-EurAgEng.
- Billingsley, J., Schoenfisch, M., 1997. The successful development of a vision guidance system for agriculture. *Comput. Electron. Agr.* 16, 147–163.
- Bossu, J., Gée, C., Jones, G., Truchetet, F., 2009. Wavelet transform to discriminate between crop and weed in perspective agronomic images. *Comput. Electron. Agr.* 65, 133–143.
- Burgos-Artizzi, X.P., Ribeiro, A., Guijarro, M., Pajares, G., 2011. Original paper: real-time image processing for crop/weed discrimination in maize fields. *Comput. Electron. Agr.* 75, 337–346.
- Dijkstra, E.W., 1959. A note on two problems in connection with graphs. *Numer. Math.* 1 (1), 269–271.
- Duda, R.O., 1972. Use of the Hough transformation to detect lines and curves in pictures. *Commun. ACM* 15, 11–15.
- Floyd, R.W., 1962. Algorithm 97: shortest path. *Commun. ACM* 5 (6), 345.
- Fontaine, V., Crowe, T.G., 2006. Development of line-detection algorithms for local positioning in densely seeded crops. *Canadian Biosyst. Eng.* 48, 7.
- García-Santillán, I., Guerrero, J.M., Montalvo, M., Pajares, G., 2017a. Curved and straight crop row detection by accumulation of green pixels from images in maize fields. *Precis. Agr.* 1–24.
- García-Santillán, I.D., Montalvo, M., Guerrero, J.M., Pajares, G., 2017b. Automatic detection of curved and straight crop rows from images in maize fields. *Biosystems Eng.* 156, 61–79.
- Gée, Ch., Bossu, J., Jones, G., Truchetet, F., 2008. Crop/weed discrimination in perspective agronomic images. *Comput. Electron. Agr.* 60, 49–59.
- Gerrish, J.B., Fehr, B.W., Van Ee, G.R., Welch, D.P., 1997. Self-steering tractor guided by computer-vision. *Appl. Eng. Agr.* 13, 559–563.
- Guerrero, J.M., Guijarro, M., Montalvo, M., Ribeiro, A., Ribeiro, A., Pajares, G., 2013. Automatic expert system based on images for accuracy crop row detection in maize fields. *Expert Syst. Appl.* 40, 656–664.
- Hague, T., Tillet, N.D., Wheeler, H., 2006. Automated crop and weed monitoring in widely spaced cereals. *Precis. Agr.* 7, 21–32.
- Hough, P.V.C., 1962. Method and means for recognizing complex patterns.
- Jiang, G., Ke, X., Du, S., Cheng, J., 2008. Detection algorithm of crop rows based on machine vision and randomized method. *Trans. Chinese Soc. Agr. Mach.* 39 (11), 85–88.
- Jiang, G., Ke, X., Du, S., Zhang, M., Cheng, J., 2009. Crop row detection based on machine vision. *Acta Opt. Sinica* 29 (4), 1015–1020.
- Jiang, G., Wang, Z., Liu, H., 2015. Automatic detection of crop rows based on multi-ROIs. *Expert Syst. Appl.* 42, 2429–2441.
- Kataoka, T., Kaneko, T., Okamoto, H., Hata, S., 2003. Crop growth estimation system using machine vision. In: IEEE/ASME International Conference on Advanced Intelligent Mechatronics, 2003. AIM 2003 Proceedings, vol. 1072, pp. b1079–b1083.
- Kise, M., Zhang, Q., 2008. Development of a stereovision sensing system for 3D crop row structure mapping and tractor guidance. *Biosyst. Eng.* 101, 191–198.
- Meyer, G.E., Neto, J.C., 2008. Verification of color vegetation indices for automated crop imaging applications. *Comput. Electron. Agr.* 63, 282–293.
- Montalvo, M., Pajares, G., Guerrero, J.M., Romeo, J., Guijarro, M., Ribeiro, A., Ruiz, J.J., Cruz, J.M., 2012. Automatic detection of crop rows in maize fields with high weeds pressure. *Expert Syst. Appl. Int. J.* 39, 11889–11897.
- Neto, J.C., 2004. A Combined Statistical-Soft Computing Approach for Classification and Mapping Weed Species in Minimum Tillage Systems. University of Nebraska, Lincoln, NE.
- Otsu, N., 1979. A threshold selection method from gray-level histogram. *IEEE Trans. Syst. Man Cybern.* 9, 62–66.
- Ribeiro, A., Fernandez-Quintanilla, C., Barroso, J., Garcia-Alegre, M.C., 2005. Development of an image analysis system for estimation of weed pressure. *Prec. Agr.* 5, 169–174.
- Romeo, J., Pajares, G., Montalvo, M., Guerrero, J.M., Guijarro, M., Ribeiro, A., 2012. Crop row detection in maize fields inspired on the human visual perception. *Sci. World J.* 2012, 484390.
- Rovira-Más, F., Zhang, Q., Reid, J.F., 2008. Stereo vision three-dimensional terrain maps for precision agriculture. *Comput. Electron. Agr.* 60, 133–143.
- Sainz-Costa, N., Ribeiro, A., Burgos-Artizzi, X.P., Guijarro, M., Pajares, G., 2011. Mapping wide row crops with video sequences acquired from a tractor moving at treatment speed. *Sensors* 11, 7059–7109.
- Si, S., Sun, X., 2015. Mathematical Modeling. National Defense Industry Press, Beijing, China.
- Si, Y.S., Jiang, G.Q., Gang, L., Rui, G., Liu, Z.X., 2010. Early stage crop rows detection based on least square method. *Trans. Chinese Soc. Agr. Mach.* 41 (7), 163–185.
- Slaughter, D.C., Giles, D.K., Downey, D., 2008. Autonomous robotic weed control systems: a review. *Comput. Electron. Agr.* 61, 63–78.
- Søgaard, H.T., Olsen, H.J., 2003. Determination of crop rows by image analysis without segmentation. *Comput. Electron. Agr.* 38, 141–158.
- Xiang, H., Tian, L., 2011. An automated stand-alone in-field remote sensing system (SIRSS) for in-season crop monitoring. *Comput. Electron. Agr.* 78 (1), 1–8 ISSN 0168–1699.
- Xu, L., Oja, E., Kultanen, P., 1990. A new curve detection method: randomized Hough transform (RHT). *Pattern Recogn. Lett.* 11, 331–338.
- Vidović, I., Cupec, R., Hocenski, Željko, 2016. Crop row detection by global energy minimization. *Pattern Recogn.* 55, 68–86.
- Woebbecke, D.M., Meyer, G.E., von Bargen, K., Mortensen, D.A., 1995. Shape features for identifying young weeds using image analysis. *Trans. Am. Soc. Agr. Eng.* 38 (1), 271–281.